MODIFIED CHARACTERISTICS-BASED SCHEMES FOR COMPRESSIBLE FLOW PAST AN AIRFOIL

A. A. Orang *

Department of Mechanical and Aerospace Engineering
Science and Research Branch, Islamic Azad University
Tehran, Iran

A. Paykani

Department of Mechanical Engineering
Parand Branch, Islamic Azad University
Parand, Iran

ABSTRACT

In this paper, the numerical study of compressible flow around an airfoil is presented. The flow is analyzed in steady state for subsonic, transonic and even in the supersonic regimes at different angles of attack. In finite-volume method convective fluxes are calculated and compared by two schemes. Modified Jameson flux scheme based on flux averaging with pressure correction is used. Modified Roe scheme which is one of the characteristics-based schemes, with modification in calculation of Jacobian matrix based on Mach number is implemented. Second-order accuracy is used with artificial dissipation to overcome numerical oscillations. The fifth-order Runge–Kutta scheme is used for time discretization. A proper boundary condition based on characteristics is applied. Numerical experiments are performed on the NACA 0012 and also NACA 4412 airfoils. The results confirm the superiority of modified upwind Roe scheme regarding the accuracy, stability and convergence. Results are compared to available results in literature and a good agreement is noticed.

Keywords: Euler equations, Compressible flow, Finite-volume method, Method of characteristics, Upwind scheme, NACA 0012 airfoil.

1. INTRODUCTION

In recent decades new and revised schemes and models are used in numerical solution of external compressible flow, so, the flow analysis around a NACA0012 symmetric airfoil is considered [1-3]. Earlier, before solving the Euler equations, potential flow was used for prediction of transonic flow with shock wave [4]. But, due to ignoring the entropy variations and production of vortices, answers with acceptable accuracy could not be expected in the upper range of transonic regime through potential equations [5]. Solving Euler equations is very useful in predicting transonic fluxes with shock waves [6]. Jameson *et al*. [1] presented numerical solution of the Euler Equations by finite volume method and combination of the artificial dissipation term by Runge-Kutta scheme for time discretization. Later, the characteristic-based (CB) method based on wave propagation was presented by Roe [2] for more efficient solution of the Euler equations. Razavi and Atashbar [7] applied incompressible version of Roe scheme to solve flow around a hydrofoil. Different methods were proposed in CFD for calculating of flux [8,9]. Today, reducing the computation time is one of the main objectives of CFD in designing of algorithms. The use of convergence accelerators to speed up convergence and reduce computation time is one of effective strategies. In steady flow problems, the number of iterations and consequently the cost of computations to achieve stable convergence can be reduced by using different techniques such as local time-stepping [10], (suggests selection of largest time-step based on the maximum Courant number), residual smoothing (averaging from residuals to increase the value of the Courant number in order to speed-up convergence, multi-grid (creating auxiliary grids to adjust the solutions of the governing equations with multistage methods in order to accelerate convergence to steady-state condition) and grid refinement [11], (smoothing grids, especially in areas with severe gradients such as near the static point and shock wave). Speeding-up the convergence to steady state by adding Enthalpy Damping has also been studied by some researchers [1,12,13]. The unstructured triangular grids were used for numerical solution of Euler Equations and concluded that this type of grid is very useful for complex domains [14]. Katz and Jameson considered a new meshless technique to solve Euler equations around an airfoil [15].

Considering the widespread use of different types of airfoil sections in aviation industry, the need to analyze and predict the behavior of fluid around the airfoils in different conditions is necessary.In this study, the NACA0012 and NACA 4412 airfoils has been selected. This paper deals with achieving accurate numerical answers in subsonic, transonic and supersonic regimes at angles of attack. Firstly, an algebraic grid with clustering near the wall is produced and then, this grid

* Corresponding author (a.atashbar@srbiau.ac.ir)

DOI : 10.1017/jmech.2012.116
Copyright © 2012 The Society of Theoretical and Applied Mechanics, R.O.C.
https://doi.org/10.1017/jmech.2012.116 Published online by Cambridge University Press

in converted to elliptical grid. Euler equations are solved using the finite volume method. Convective terms are calculated using two schemes; first, modified Jameson flux scheme and, second, modified Roe schemes. Appropriate boundary conditions based on the characteristics are applied and their effect on the solution of the problem is investigated. It also has been done for NACA 4412 airfoil. One of the main objectives of this study is optimization of the flux calculations and, consequently, improvement of accuracy, reduction of computation time or in other words cost reduction and the other is capturing vortices with no existence of viscous effects.

2. GOVERNING EQUATIONS

The governing two-dimensional equations for inviscid compressible flow include equations of continuity, momentum in the x and y directions and the energy equation. Equations should be written in conservative form for numerical solution, so, following equations are obtained [16]:

$$\frac{\partial}{\partial t}\iint_{\Omega} U dA + \oint_{\partial\Omega} F_N \, dL = 0 \tag{1}$$

$$U = \begin{bmatrix} \rho \\ \rho u \\ \rho v \\ \rho E \end{bmatrix}, \quad F_N = \begin{bmatrix} \rho u_n \\ \rho u_n + p \cos\zeta \\ \rho v u_n + p \sin\zeta \\ \rho u_n H \end{bmatrix} \tag{2}$$

$$H = E + \frac{p}{\rho} \quad \sin\zeta = -\frac{\Delta x}{\Delta L} \quad \cos\zeta = \frac{\Delta y}{\Delta L} \tag{3}$$

$$\Delta L = \sqrt{\Delta x^2 + \Delta y^2}, \quad \vec{N} = \cos\zeta \vec{i} + \sin\zeta \vec{j},$$
$$u_n = u\cos\zeta + v\sin\zeta, \quad u_t = v\cos\zeta - u\sin\zeta \tag{4}$$

where u_n, u_t, ΔL, $\vec{N}$ are normal and parallel components of velocity, length and the normal unit vector or the direction of virtual wave propagation respectively as shown in Fig. 1.

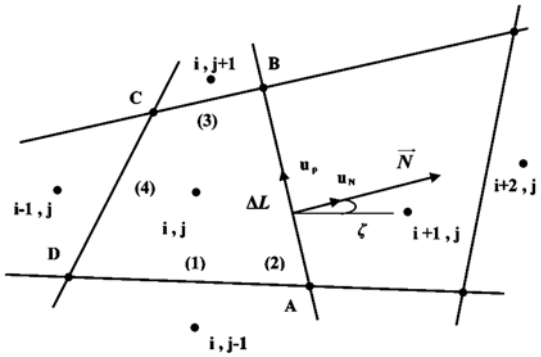


Fig. 1 Schematic representation of the primary cell to evaluate normal convective fluxes

2.1 Convective Fluxes

Two schemes were used to evaluate convective fluxes at any cell side, while the first-order derivatives of left and right cells were averaged. Considering Figure1, one has:

$$\oint_{\delta\Omega} F_N \, dL = \sum_{K=1}^{4} F_N{}^{(K)} \Delta L \tag{5}$$

where, K is attributed to each cell side. Two schemes to calculate convective fluxes (FN) at primary cell interfaces like AB in Figure1 were utilized as expressed below:

2.1.1 Modified Jameson Flux Scheme

A major problem in the averaging scheme is its tendency to odd even decoupling [1-14]. To solve this problem, according to the fluid flow behavior, we notice for the solution of fluxes by physical evidence. Here, first- and second-order pressure-based flux weighting factors are defined with biasing the convective flux terms. The values of two neighboring cells are used which has first-order accuracy. Hence considering Fig. 1:

$$\xi_{AB} = \frac{P_{i,j}}{P_{i,j} + P_{i+1,j}} \tag{6}$$

For obtaining higher accuracy, more cells should be utilized. Corresponding flux weighting factors are proposed as:

$$\xi_{AB-L} = \frac{P_{i-1,j}}{P_{i,j} + P_{i-1,j}}, \quad \xi_{AB-R} = \frac{P_{i,j}}{P_{i,j} + P_{i+1,j}},$$
$$\xi_{AB} = \frac{\xi_{AB-L} + \xi_{AB-L}}{2} \tag{7}$$

According to the above coefficient, conservative variables at AB interface are calculated as following:

$$U_{AB} = \xi_{AB} U_{i,j} + (1 - \xi_{AB}) U_{i+1,j} \tag{8}$$

Then fluxes through AB face will be assigned. Based on the boundary conditions and fluid flow behavior, ξ can act as a downwasher or upwasher. A similar procedure is followed for other sides. These factors come from the fact that the macroscopic pressure, p, acts as a driving force for flow between the cells [6].

2.1.2 Modified Upwind Roe Scheme

Roe upwind scheme is based on the propagation of acoustic waves and characteristics. According to the Eq. (2), after obtaining of Jacobian matrix, the corresponding eigenvalues and right-hand side eigenvectors will be:

https://doi.org/10.1017/jmech.2012.116 Published online by Cambridge University Press

$$\hat{\lambda}_i = \begin{pmatrix} \hat{u}_n - \hat{a} \\ \hat{u}_n \\ \hat{u}_n \\ \hat{u}_n + \hat{a} \end{pmatrix},$$

$$\hat{R}_i = \begin{pmatrix} 1 & 0 & 1 & 1 \\ \hat{u} - \hat{a}\cos\zeta & -\hat{a}\sin\zeta & \hat{u} & \hat{u} + \hat{a}\cos\zeta \\ \hat{v} - \hat{a}\sin\zeta & \hat{a}\cos\zeta & \hat{v} & \hat{v} - \hat{a}\sin\zeta \\ \widehat{H} - \widehat{u_n}\,\hat{a} & \hat{u}_t\,\hat{a} & \frac{\hat{u}^2 + \hat{v}^2}{2} & \widehat{H} + \widehat{u_n}\,\hat{a} \end{pmatrix} \quad (9)$$

Wave's strength indicates jump discontinuity. They are difference of characteristic quantities between two cells:

$$\hat{\delta}_i = \begin{pmatrix} \frac{\Delta p - \hat{\rho}\hat{a}\,\Delta u_n}{2\hat{a}^2} \\ \frac{\hat{\rho}\,\Delta u_t}{\hat{a}^2} \\ \Delta\rho - \frac{\Delta p}{\hat{a}^2} \\ \frac{\Delta p + \hat{\rho}\hat{a}\,\Delta u_n}{2\hat{a}^2} \end{pmatrix} \quad (10)$$

Then considering Fig. 1 the flux in AB interface will be calculated according to Eq. (11):

$$F_N = 0.5(F_{NR} + F_{NL}) - 0.5\sum_{k=1}^{4} |\hat{\lambda}_{(k)}|\,\hat{\delta}_{(k)}\,\hat{R}^{(k)} \quad (11)$$

where a is sound speed and hatted quantities are average values of two interacted cells which various methods have been used for calculation of them, Roe proposed the following parameters which is known as original Roe averaging [2]:

$$\hat{\rho} = \sqrt{\rho_L\,\rho_R}$$
$$\hat{u} = \frac{\sqrt{\rho_L}\,u_L + \sqrt{\rho_R}\,u_R}{\sqrt{\rho_L} + \sqrt{\rho_R}}$$
$$\hat{v} = \frac{\sqrt{\rho_L}\,v_L + \sqrt{\rho_R}\,v_R}{\sqrt{\rho_L} + \sqrt{\rho_R}}$$
$$\widehat{H} = \frac{\sqrt{\rho_L}\,H_L + \sqrt{\rho_R}\,H_R}{\sqrt{\rho_L} + \sqrt{\rho_R}} \quad (12)$$

Modified upwind Roe scheme proposes an averaging method based on local Mach number. Considering Fig. 1 for first-order accuracy we have:

$$\xi_{AB} = \frac{Mach_{i,j}}{Mach_{i,j} + Mach_{i+1,j}}, \quad Mach_{i,j} = \frac{V_{i,j}}{a_{i,j}},$$
$$a_{i,j} = \sqrt{\gamma\frac{p_{i,j}}{\rho_{i,j}}} \quad (13)$$

and for second-order accuracy:

$$\xi_{AB-L} = \frac{Mach_{i-1,j}}{Mach_{i,j} + Mach_{i-1,j}},$$
$$\xi_{AB-R} = \frac{Mach_{i-j}}{Mach_{i,j} + Mach_{i+1,j}},$$
$$\xi_{AB} = \frac{\xi_{AB-L} + \xi_{AB-R}}{2} \quad (14)$$

According to the above coefficient, hatted quantities at AB interface are calculated as following:

$$\hat{U}_{AB} = \xi_{AB}\,U_{i,j} + (1 - \xi_{AB})\,U_{i+1,j} \quad (15)$$

Mach number has a significant role in propagation of information in compressible flows and applying these weighting factors for upwind schemes such as Roe scheme improve the behavior of main upwind Roe scheme regarding accuracy and convergence.

2.2 Second-Order Accuracy

In current work, second-order accuracy is used. Considering Fig. 1, to achieve second-order accuracy for AB interface we have:

$$U_L = 1.5U_{i,j} - 0.5U_{i-1,j}, \quad U_R = 1.5U_{i+1,j} - 0.5U_{i+2,j} \quad (16)$$

To avoid numerical oscillations artificial dissipation is added in both schemes. Then the main equations will be:

$$\frac{d}{dt}(A_{i,j}\,U_{i,j}) + Q(U_{i,j}) - D(U_{i,j}) = 0 \quad (17)$$

where Q includes the discretized form of integral convective terms. $D(U_{i,j})$ can depreciate all adverse oscillations in the vicinity of the shock wave. A number of different numerical approaches suggest that a combination of second-order and fourth-order differential terms is very efficient for artificial dissipation [1]:

$$DU = D_x U + D_y U \quad (18)$$

$$D_x U = d_{i+\frac{1}{2},j} - d_{i-\frac{1}{2},j}$$
$$D_y U = d_{i,j+\frac{1}{2}} - d_{i,j-\frac{1}{2}} \quad (19)$$

$$d_{i+\frac{1}{2},j} = \frac{A_{i,j}}{\Delta t}\left[\varepsilon^{(2)}_{i+\frac{1}{2},j}(U_{i+1,j} - U_{i,j}) - \varepsilon^{(4)}_{i+\frac{1}{2},j}(U_{i+2,j} - 3U_{i+1,j} + 3U_{i,j} - U_{i-1,j})\right] \quad (20)$$

$\varepsilon^{(2)}$ and $\varepsilon^{(4)}$ coefficients are defined based on pressure [1]:

$$\upsilon_{i,j} = \frac{|\,p_{i+1,j} - 2p_{i,j} + p_{i-1,j}\,|}{|\,p_{i+1,j}\,| + 2|\,p_{i,j}\,| + |\,p_{i-1,j}\,|} \quad (21)$$

https://doi.org/10.1017/jmech.2012.116 Published online by Cambridge University Press

$$\varepsilon^{(2)}_{i+\frac{1}{2},j} = k^{(2)} \max(\upsilon_{i+1,j},\ \upsilon_{i,j})$$
$$\varepsilon^{(4)}_{i+\frac{1}{2},j} = \max\left(0, k^{(4)} - \varepsilon^{(2)}_{i+\frac{1}{2}}\right) \quad (22)$$

The general and fixed values can be used as $k^{(2)} = 1/4$ and $k^{(4)} = 1/256$. Since υ is related to sharp pressure gradients, the value of $\varepsilon^{(2)}$ is higher and $\varepsilon^{(4)}$ equals zero. But in other areas without shock wave or the static points, the value of $\varepsilon^{(2)}$ is negligible and dissipation is applied only in fourth-order. For modified Jameson flux scheme adding artificial dissipation is necessary even at first-order scheme but for upwind Roe scheme at second-order accuracy, it is added weakly avoiding numerical oscillations.

3. TIME DISCRETIZATION AND BOUNDARY CONDITIONS

3.1 Time Discretization

The fourth-order and fifth-order Runge - Kutta schemes are considered in numerical solutions because of wider stability range. Since the RK5 has a higher stability range (CFL ≤ 4), it has been used for time discretization in the present study:

$$\frac{\partial U}{\partial t} + Q^*(U) = 0,\ U^{(n+1)} = U^{(n)} - \varepsilon_m\, \Delta t Q^{*(n)}(U)\ ,$$
$$\varepsilon_m = 1/4, 1/6, 3/8, 1/2, 1.\ (m = 1,\ ....5) \quad (23)$$

where Q^* is total residual including convective and dissipation terms. This time-stepping proved its superiority when compared to other methods such as the simple Euler method. The number of iterations to achieve steady state is reduced by using a variable time step that depends on the local flow changes and the grid spacing as [7-17]

$$\Delta t = \mathrm{Max}\left(\frac{CFL \times \mathrm{Min}(\sqrt{\Delta x^2_{i,j} + \Delta y^2_{i,j}})}{\mathrm{Max}[a + \sqrt{u^2_{i,j} + v^2_{i,j}}]}, \frac{CFL}{\mathrm{Max}_n(\gamma_n)}\right)$$
$$\gamma_n = \mathrm{Max}\left\{\left(|\lambda_{(1)}|\ ,\ |\lambda_{(2)}|\ ,\ |\lambda_{(3)}|\ ,\ |\lambda_{(4)}|\right)\sqrt{\Delta x^2_{i,j} + \Delta y^2_{i,j}}\right\}\ ,$$
$$n = 1,\ 2,\ 3,\ 4 \quad (24)$$

3.1.1 Residual Definition

Residual at each time step is the largest value of difference between density, velocity and pressure which are averaged in cells of domain:

$$Enorm = \mathrm{Max}\left((\rho^{n+1} - \rho^n)\ ,(V^{n+1} - V^n)\ ,(P^{n+1} - P^n)\right) \quad (25)$$

3.2 Boundary Conditions

3.2.1 Solid Boundary Condition

A proper solid boundary condition should overcome the dissipation without any reflection [18,19]. A characteristic of the domain does not flow in solid boundary, so, a physical boundary condition is necessary. This condition is extended by means of eliminating perpendicular component of velocity in wall:

$$q_{\perp b} = \overline{V} \cdot \overline{n} = 0 \quad (26)$$

Based on one-dimensional characteristics consistent equations, we have:

$$dc_1 = dp - \rho a du_n = 0$$
$$dc_2 = dp - a^2 d\rho = 0 \quad (27)$$
$$dc_3 = dp + \rho a du_n = 0$$

In solid boundaries, dc_1 and dc_2 waves propagate towards these boundaries, after discretization we obtain:

$$p_{ij} - p_b - \rho_{ij}\, a_{ij}(u_{ij,n} - u_{b,n}) = 0$$
$$p_{ij} - p_b - a^2_{ij}\ (\rho_{ij,n} - \rho_{b,n}) = 0 \quad (28)$$

where, u_b is the value on the solid boundary. In solid surface $u_{b,n} = 0$. By combining the above equations we have:

$$p_b = p_{ij} - \rho_{ij}\, a_{ij}\, u_{ij,n}$$
$$\rho_b = \rho_{ij} + \frac{u_{ij,n}}{a_{ij}}\ \rho_{ij} \quad (29)$$

3.2.2 Far Field Boundary Condition

For far field, the aim is to minimize reflections of forced dissipations. We consider the perpendicular flow on this boundary and assume that the position is one-dimensional. The fixed and extrapolated Riemann variables can be obtained as following [18]:

$$R_\infty = u_{\infty n} + \frac{2}{\gamma - 1}\ a_\infty$$
$$R_e = u_{en} + \frac{2}{\gamma - 1} a_e \quad (30)$$

Vertical velocity and sound speed are calculated as following:

$$u_n = \frac{1}{2}(R_e + R_\infty)$$
$$a = \frac{\gamma - 1}{4}(R_e - R_\infty) \quad (31)$$

Two independent conditions are required to complete the far field boundary conditions which are obtained through tangential velocity component and entropy.

4. CONVERGENCE ACCELARATION TECHNIQUES

In steady flow calculations, convergence acceleration techniques are incorporated into the scheme to increase the convergence rate to steady state. The techniques used in the present work may be briefly described as follows:

https://doi.org/10.1017/jmech.2012.116 Published online by Cambridge University Press

4.1 Local Time Stepping

In unsteady flow calculations, the time-step has to be the same everywhere in the calculation domain. However, for steady flow calculations, since the transients are valueless, the solution can be allowed to advance at the maximum rate within each cell compatible with a fixed CFL and size of the cell. The time-steps will differ from one point to another as a function of local propagation speeds and corresponding local CFL condition. The solution will progress in time towards the steady state at different pace at each point. However, convergence will still depend on the slowest progressing zone.

4.2 Enthalpy Damping

Following Jameson *et al.* [1], an enthalpy damping term of the form, $\beta(H - H_\infty)\,\underline{U}$ can be added to the set of equations, which will have the effect of accelerating the convergence towards the acceptable tolerance. This does not affect the steady state solution as at steady state, $H \to H_\infty$. The residual Q in Eq. (23) is replaced by:

$$\tilde{Q}(U_{i,j}) = Q^*(U_{i,j}) + \beta(H_{i,j} - H_\alpha)\, U_{i,j} \qquad (32)$$

However, Jameson *et al.* [1] have observed that the use of ρE or ρH in the energy equation would give a quadratic term which can have a destabilizing effect. So, $U_{i,j}$, in second term of the right hand side of Eq. (32) is replaced by $\tilde{U}_{i,j}$, where:

$$\tilde{U}_{i,j} = \begin{pmatrix} \rho \\ \rho u \\ \rho v \\ 1 \end{pmatrix} \qquad (33)$$

It is found that β of 0.0025 gave the best results.

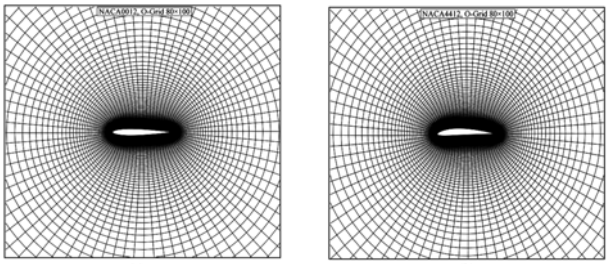
5. NUMERICAL RESULTS AND DISCUSSION

Numerical tests are performed with subsonic, transonic and supersonic flows at angles of attack over NACA0012 and NACA4412 airfoils. Utilizing modified Roe scheme, we can increase angle of attack to higher value even 90°. The grid consist of 110 × 70 cells along radial and environmental direction, respectively, and 15 chord lengths away from airfoil for outer boundary as shown in Fig. 2.

To see the effect of grid size on results, grid independence testing is done in transonic flow for three different grids using modified Roe scheme (Fig. 3). It can be observed that refining the grid does not cause significant changes in the distribution of Mach number and applying 110 × 70 grid is acceptable.

5.1 Subsonic Flow

To validate performance of present work, numerical tests were conducted with different Mach numbers in



(a) (b)

Fig. 2 Grid for (a) NACA 0012 (b) NACA 4412 airfoil

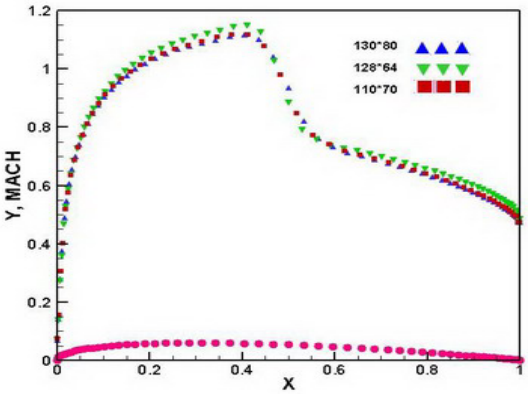


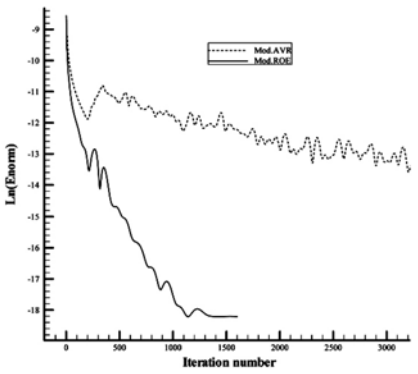
Fig. 3 Grid independence analysis in transonic regime (modified Roe)

the case of compressible inviscid flow around a NACA 0012 and NACA 4412 airfoils. One case was studied at Mach = 0.63 and AOA = 2° and the other for Mach = 0.5 and AOA = 3°. In Fig. 4, convergence history, for these cases have been shown. Comparison of convergence history between original Roe and modified Roe schemes for those cases is illustrated in Fig. 5. It is obvious that Mod.ROE is faster in convergence rate. The second-order accuracy is used and artificial dissipation is applied. It is shown that modified Roe (Mod.ROE) scheme result in a faster convergence which demonstrates its capability to handle compressible flows. The wall pressure distribution for Mach = 0.63, AOA = 2° is compared to that of AGARD report No.575 [3] in Fig. 6. Wall pressure distribution for other subsonic case with Mach = 0.5, AOA = 3° is plotted in Fig. 7. It is closely comparable to that of Katz and Jameson [15]. For Mod.AVR the CFL number is equal to 1 and for Mod.ROE, was 3.

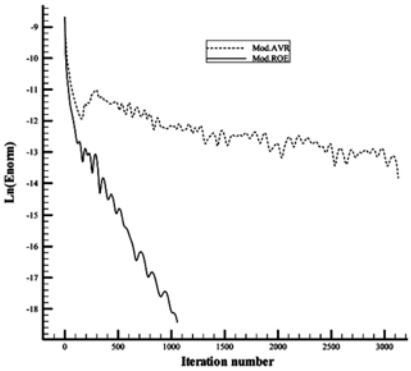
Comparison of Mach number distribution for Mach = 0.5, 0.6, 0.7 and AOA = 0° is depicted in Fig. 8 with Mod.ROE scheme. As shown in the Fig. 8, the subsonic flow passed over the NACA 0012 airfoil and does not reach the sonic speed. As can be seen, the flow is subsonic even in M = 0.7 and does not still reach the transonic range. Pressure coefficient contours are shown in Fig. 9 at three different Mach numbers.

Another test case in subsonic flow is NACA 4412 airfoil. In Fig. 10 the pressure contour and Mach number distribution for this airfoil in Mach = 0.63 and AOA = 3° is plotted with Mod.ROE scheme.

https://doi.org/10.1017/jmech.2012.116 Published online by Cambridge University Press

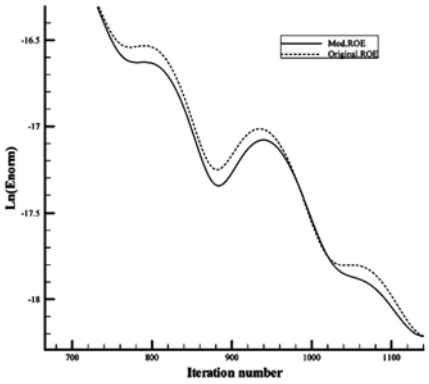


(a)

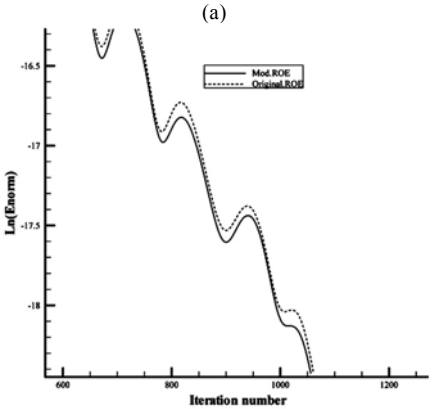


(b)

Fig. 4 Comparison of convergence history, NACA 0012, (a) Mach = 0.63, AOA = 2°, (b) Mach = 0.5, AOA = 3°. Mod.JMS, modified Jameson; Mod.ROE, modified Roe



(a)



(b)

Fig. 5 Comparison of convergence history, NACA 0012, (a) Mach = 0.63, AOA = 2°, (b) Mach = 0.5, AOA = 3°. Mod.ROE, modified Roe; Original.ROE, original Roe

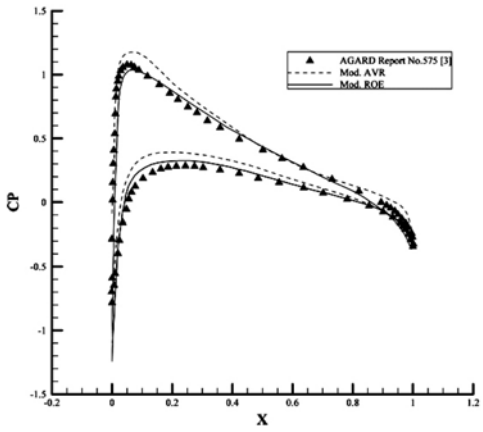


Fig. 6 Wall pressure coefficient, Mach = 0.63, AOA = 2°, NACA 0012, Mod.JMS, modified Jameson; Mod.ROE, modified Roe

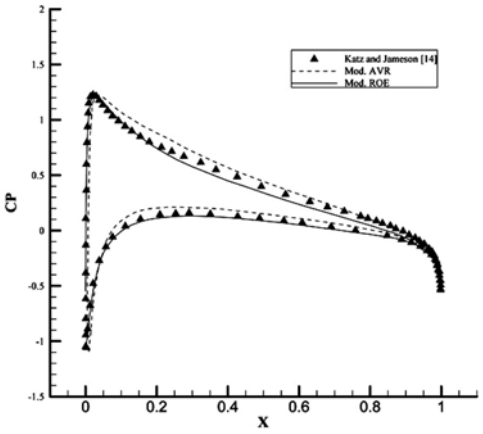


Fig. 7 Wall pressure coefficient, Mach = 0.5, AOA = 3°, NACA 0012, Mod.JMS, modified Jameson; Mod.ROE, modified Roe

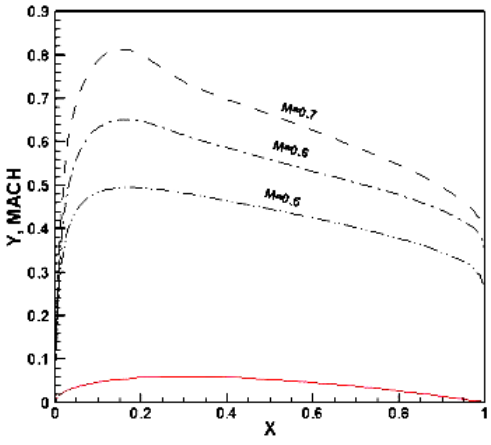
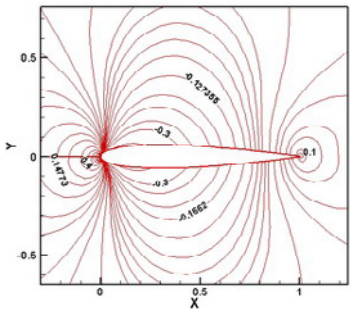
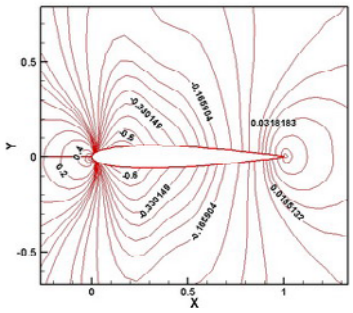


Fig. 8 **Comparison of Mach number distribution along NACA 0012 airfoil at three subsonic Mach number**s, Mod.Roe

https://doi.org/10.1017/jmech.2012.116 Published online by Cambridge University Press





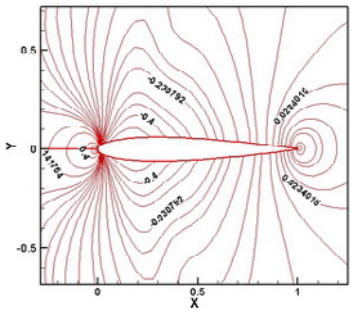
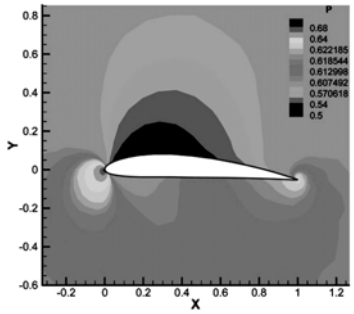


Fig. 9 **Pressure coefficient contours** at three subsonic Mach numbers for NACA 0012, Mod.Roe



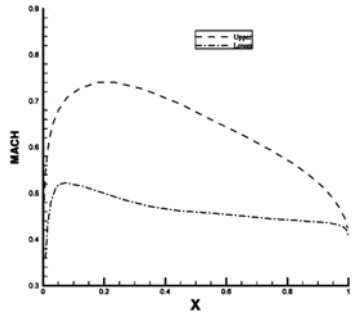


Fig. 10 (a) **Pressure contours** (b) Mach number **distribution for** NACA 4412, Mach = 0.63, AOA = 2°, Mod.ROE

In Fig. 11 streamlines for Mach = 0.63 and angles of attack with Mod.ROE scheme are presented for NACA 0012. It is obvious that increasing the angle of attack rises the pressure difference between upstream and downstream where by causing the separation at angles higher than 10°. Although viscosity is absent in Euler equations because of two factors the flow field is rotational according to Corocco's theorem. One is entropy increasing behind the shock wave and the other is heat transfer which is modeled in Euler equations. In wake region vortices are appeared which approach to leading edge by increasing the angle of attack. Vector plot of Mod.ROE at Mach = 0.63 and AOA = 16° is demonstrated in Fig. 12.

By increasing the angle of attack on the airfoil, lift coefficient increases up to reach to stall point. Table 1 represents the lift coefficient for NACA 0012 in Mach = 0.63 at different angles of attack.

5.2 Transonic Flow

By increasing the velocity of the flow, this type of flow regime reaches to sonic and supersonic ranges along with the shock wave. Figure 13 illustrates convergence history comparison between ModAVR and Mod.ROE schemes for NACA 0012 in Mach = 0.85 and AOA = 1°. As seen again, Mod.ROE scheme has a faster convergence in comparison with Mod.AVR. In Fig. 14 wall pressure coefficient distribution is compared with that of Katz and Jameson [15]. Good agreement can be seen in Mod.ROE scheme. As shown, shock wave is occurred at 0.85 and 0.6 of chord from leading edge in upper and lower surface respectively.

Figure 15 demonstrates the comparison of Mach number distribution on the NACA0012 airfoil in Mach numbers of 0.8, 0.85 and 0.9 with AOA = 0° using Mod.ROE scheme. It is clear that as the Mach number increases the shock wave moves toward the airfoil trailing edge.

5.3 Supersonic Flow and Very High Angles of Attack

To demonstrate high stability of Mod.ROE scheme, it was implemented to supersonic flow and also very high angle of attack even AOA = 90° in different flow regimes. For supersonic case NACA 0012 in Mach = 1.2 was tested. Pressure contour for this case is presented in Fig. 16 and the Bow shock in front of the airfoil can be observed. In Fig. 17 pressure contours and streamlines for NACA 0012 are illustrated in AOA = 90° and Mach = 0.5, 0.85, 1.2. Strong vortices can be seen at downstreams.

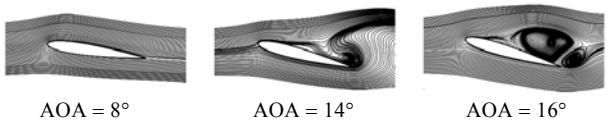
6. CONCLUSIONS

Considering the widespread use of different types of airfoil sections in aviation industry, the need to analyze and predict the behavior of fluid around the airfoils in

https://doi.org/10.1017/jmech.2012.116 Published online by Cambridge University Press

Table 1 Lift coefficient at different angles of attack for M = 0.63, Mod.Roe

α	2	4	6	8	10	12	14	16	18
C_L	0.3227	0.6443	0.9008	1.0610	1.2396	1.3563	1.4278	1.4657	1.4505



AOA = 8° AOA = 14° AOA = 16°

Fig. 11 Stream lines with angles of attack, Mach = 0.63, NACA 0012, Mod.Roe

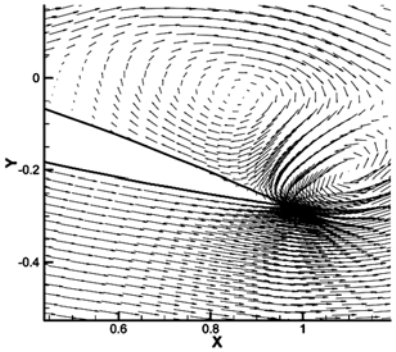


Fig. 12 Vector plot, Mach = 0.63, AOA = 16°, NACA 0012, Mod.ROE

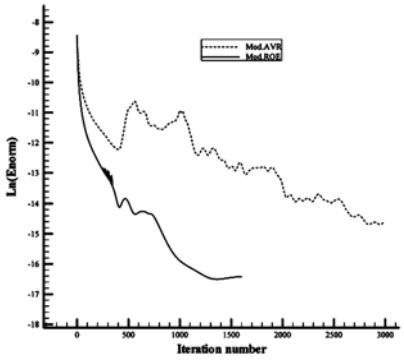


Fig. 13 Comparison of convergence history, Mach = 0.85, AOA = 1°. NACA 0012, Mod.JMS, modified Jameson; Mod.ROE, modified Roe

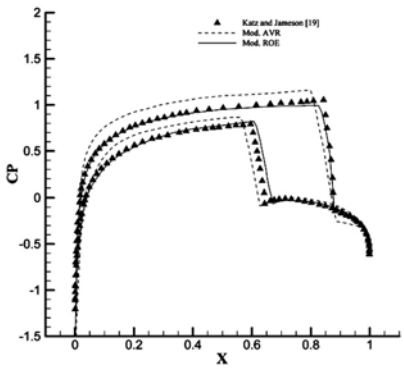


Fig. 14 Wall pressure coefficient, Mach = 0.85, AOA = 1°, NACA 0012, Mod.JMS, modified Jameson; Mod.Roe, modified Roe

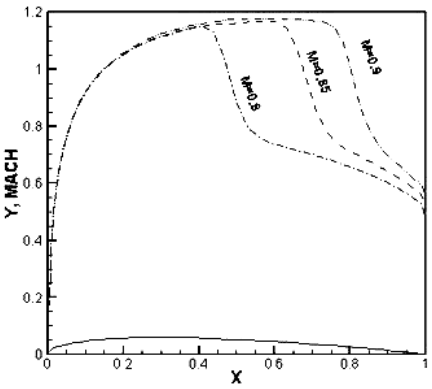


Fig. 15 Comparison of Mach number distribution in three transonic flows, NACA 0012, AOA = 0°, Mod.Roe

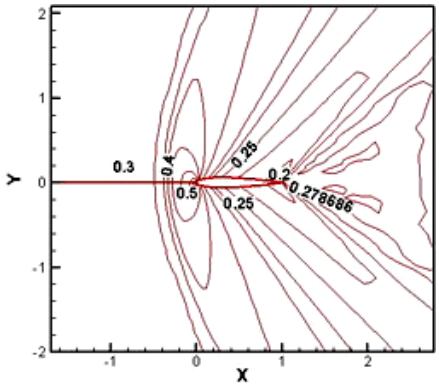
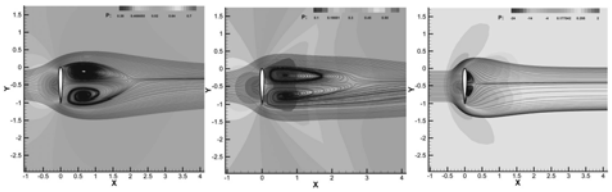


Fig. 16 Pressure contour for NACA 0012, Mach = 1.2, AOA = 0°, Mod.Roe



Mach = 0.5 Mach = 0.85 Mach = 1.2

Fig. 17 **Pressure contours** and streamlines **for** NACA 0012, AOA = 90°, Mod.Roe

different conditions is necessary. In present work, two schemes which are weighted averaging called modified Jameson scheme and modified Roe scheme, were adopted to solve compressible flows over NACA 0012 and NACA 4412 airfoils in subsonic, transonic and supersonic regimes at angles of attack. Time discretization, was done by fifth-order Runge-Kutta scheme. Local time stepping and enthalpy damping were utilized to accelerate convergence process. In convective flux treatment, the propagation of information along characteristics was taken into account. The schemes based on the propagation of information along characteristics with modification in Jacobian matrix, allow relatively high CFL numbers and have high convergence rate with less numerical oscillations. The Mod.ROE scheme was applied to the airfoil problem at high angles of attack. Applying artificial dissipation in schemes resulted in capturing

https://doi.org/10.1017/jmech.2012.116 Published online by Cambridge University Press

vortices with absence of viscous effects. Appropriate boundary conditions based on characteristics were applied and their effect on the solution of the problem was investigated. Flow around NACA 0012 airfoil was investigated by those methods. The obtained answers are compared by the results of other researchers and are quite acceptable in terms of accuracy. The substantial consensus was achieved utilizing Mod.ROE method particularly even at high Mach number and angles of attack.

REFERENCES

1. Jameson, A., Schmidit, W. and Turkel, E., "Numerical Solutions of the Euler Equations by Finite Volume Methods Using Runge-Kutta Time-Stepping," *AIAA 14th Fluid and Plasma Dynamics Conference. Palo Alto*, California, June, pp. 23–25 (1981).
2. Roe, P. L., "Characteristic-Based Schemes for the Euler Equations," *Annual Review of Fluid Mechanics*, **18**, pp. 337–365 (1986).
3. Lock, R. C., "Test Case for Numerical Methods in Two-Dimensional Transonic Flows," *AGARD REPORT* (1970).
4. Jamson, A., "Numerical Calculation of Transonic Flow with Shock Waves," *Symposium Transsonicum*, Gottingen, Springer-Verlag (1976).
5. Rizzi, A. and Vivand, H., "Numerical Methods for the Computation of Inviscid Transonic Flow with Shocks," *Proceeding of GAMM Workshop*, Stockholm, Viewveg verlag (1981).
6. Razavi, S. E., Ghasemi, J. and Farzadi, A., "Flux Modeling in the Finite-Volume Lattice Boltzmann Approach," *International. Journal of Computational Fluid Dynamics*, **23**, pp. 69–77 (2009).
7. Razavi, S. E. and Atashbar, O. A., "A Comparative Investigation of Hydrofoil at Angles of Attack," *International. Journal of Numerical Methods Fluids*, **69**, pp. 1087–1101 (2012).
8. Pan, D. and Cheng, J. C., "Upwind Finite Volume Navier-Stokes Computations on Unstructured Triangular Meshes," *AIAA Journal*, p. 31 (1993).
9. Lyra, P. R. M., Morgan, K., Peraire, J. and Perio, J., "TVD Algorithms of the Compressible Euler Equations on Unstructured Meshes," *International Journal of Numerical Methods in Fluids*, **19** pp. 827–847 (1994).
10. Razavi, S. E., Barar, F. and Farhangmehr, V., "Characteristic-Based Finite Volume Solution for Natural Convection Around Horizontal Cylinder," *Journal of Applied Science*, **8**, pp. 1905–1911 (2008).
11. Nakamura, S. and Holst, T. L., "A New Solution-Adaptive Grid Generation Method for Transonic Airfoil Flow Calculations," *NASA Technical Memorandum*, 81330 (1981).
12. Rizzi, R. L. and Eriksson, E., "Transfinite Mesh Generation and Damped Euler Equation Algorithm for Transonic Flow Around Wing-Body Configuration," *5th AIAA Computational Fluid Dynamics Conference*, Palo Alto (1981).
13. Vivand, H., "Pseudo Unsteady Methods for Transonic Flow Computation," *Proceedings of 7th International Conference on Numerical Methods in Fluid Dynamic*, Stanford, (1980).
14. Jameson, A. and Mavriplis, D., "Finite Volume Solution of the Two-Dimensional Euler Equations on a Regular Triangular Mesh," *AIAA 23rd Aerospace Sciences Meeting, Reno*, Nevada, January, pp. 14–17 (1985).
15. Katz, A. and Jameson, A., "Meshless Scheme Based on Alignment Constraints," *AIAA Journal*, **48**, pp. 2501–2511 (2010).
16. Hoffman, A. K. and Chiang, S. T., *Computational Fluid Dynamics for Engineers*, McGraw-Hill, New York (1994).
17. Swanson, R. C., Turkel, E. C. and Rossow, C., "Convergence Acceleration of Runge-Kutta Schemes for Solving the Navier-Stokes Equations," *Journal of Computational Physics*, **224**, pp. 365–388 (2007).
18. Mirzaee, B., Khoshravan, E. and Razavi, S. E., "Finite-Volume Solution of a Cylinder in Cross Flow with Heat Transfer," *International. Journal of Engineering*, **15**, pp. 303–314 (2002).
19. Mazaheri, K. P. and Roe, L., "New Light on Numerical Boundary Conditions," *AIAA 10th Computational Fluid Dynamics Conference, Honolulu*, HI (1991).

(Manuscript received September 2, 2011, accepted for publication March 19, 2012.)

https://doi.org/10.1017/jmech.2012.116 Published online by Cambridge University Press